Pergamon

Cement and Concrete Research 31 (2001) 1573–1579

CEMENT AND CONCRETE RESEARCH

Early ages shrinkage mechanisms of ultra-high-performance cement-based materials

A. Feylessoufi[a,*], F. Cohen Tenoudji[b], V. Morin[b], P. Richard[a]

[a]*Centre de Recherche sur les Matériaux Cimentaires (CRMC), University of Evry, Boulevard François-Mitterrand, F-91025 Evry cedex, France*
[b]*Laboratoire Universitaire des Applications de la Physique (LUAP), University of Paris VII, 4, place Jussieu, F-75005 Paris, France*

Received 12 October 1999; accepted 6 July 2001

Abstract

Early age chemical and microstructural evolution of an ultra-high-performance cement-based material is analyzed by autogeneous shrinkage monitoring simultaneously with ultrasonic propagation measurements. The hydration progress is determined with a calorimetric equipment. The combined analysis with these complementary methods leads to the identification of five stages in this evolution: (1) a settling period with short-range reorganization without any cluster formation or shear resistance; (2) an aggregation period with unconnected clusters formation and growing leading to the percolation of solid particles; (3) a postpercolation bond development phase leading to a globally structured framework; (4) a progressive reinforcement by multiplication of connections within the framework leading to a fully hyperstatic state; (5) a hyperstatic phase where all the particles are connected, with the consolidation by pores filling.

Keywords: Concrete; Reactive powder concrete; Ultrasonic spectroscopy; Shrinkage; Percolation

1. Introduction

Phase morphology in heterogeneous cementitious materials has a great importance in microcrack formation mechanisms during setting. This importance becomes greater when chemical reactions cause local shrinkage or important variation in phase network or in matrix moduli evolution, provoking strain incompatibility inside the material.

This paper focuses on this problem by studying a cement-based material belonging to a family of ultra-high-performance concrete, namely reactive powder concrete (RPC). These concretes have been elaborated by the concomitant improvement of several parameters such as particle-size homogeneity, porosity and microstructure. Compressive strengths ranging between 200 and 800 MPa, fracture energies between 1200 and 40,000 J/m^2 and ultimate tensile strain before fracture of the order of 1% are reached [1]. This was achieved by reducing the size of the largest aggregates, lowering the CaO-to-SiO_2 ratio by the introduction of silica components, lowering the water-to-cement ratio by superplasticizers and, for special uses, pressing or introducing reactive quartz into formula. High-temperature curing led to further and more dramatic improvement.

Recent research works have analyzed the effects of porosity distribution [2,3], of silicate hydrates shape modifications [4,5] or of the pressure application during treatments [6] for a better understanding of the enhancement of mechanical properties of ultra-high-performance cement-based materials. However, the main parameter seems to be the granular classes separation, which allows local shrinkage during setting by the separation of larger particles with an excess amount of smaller particles making possible their concomitant rearrangement during the shrinkage.

In this paper, this crucial period is focused upon, with the goal of a better understanding of ordering the different structuration mechanisms of the medium. On one hand, the autogeneous shrinkage and structuration mechanisms are intimately linked and, on the other hand, this shrinkage corresponds to the practical situation of the concrete in the shuttering (casting process). This is a combined methodology with simultaneous measurements of early age autogeneous shrinkage and calorimetry, which are used here with a suited spectrometric ultrasonic technique.

* Corresponding author. Tel.: +33-169-47-77-11; fax: +33-169-47-77-12.
E-mail address: a.feylessoufi@physique.univ-evry.fr (A. Feylessoufi).

0008-8846/01/$ – see front matter
PII: S0008-8846(01)00602-0

Indeed, the recent development of the latter technique [7] has given us the capability to reach the different levels of particle organization, and new enlightenment on the physics of the phenomena can be brought out.

2. Experimental

2.1. Material

The RPC considered here is prepared from the following components expressed in mass ratio with respect to cement: Type V Portland cement; fine quartz sand, 150–400 μm (1.1); undensified silica fume, with specific surface of 18 m^2/g (0.25); acrylic superplasticizer (0.018); water (0.16). The components are mixed, cast and vibrated like a conventional concrete. Dry concrete powder components are mixed for 3–5 min, water is added with half of the volume of the superplasticizer and mixed for 3 min, the last half of the volume of the superplasticizer is added and mixed for 5 min. This last water introduction marks the start of time (hour 0). The same mixture is degassed and immediately divided into three different samples for shrinkage, acoustic and calorimetric experiments.

2.2. Calorimetric monitoring and hydration degree parameter determination

Calorimetric measurements were made in order to calculate the hydration degree of the concrete specimen under specified external temperature conditions.

The reactions being exothermic, a sample with a large size would have its temperature increase strongly during the setting. In the method used here, one attempts to limit this temperature increase to 1–2°C at most by putting a sample of small size in an isothermal bath. This is why this calorimetric method is so-called 'isothermal calorimetry'. The dissipated heat power is deduced from the small temperature difference ΔT between the heart of the sample and its exterior.

The dissipated power is then expressed by the addition of two terms: the first one is the product of the mean thermal conductance of the sample and its container by the temperature difference ΔT; the second term is proportional to the product of the mean calorific capacitance by the time derivative of the temperature difference $d(\Delta T)/dt$. These two mean values are obtained from two calibration measurements. One can then obtain the dissipated heat power and the dissipated heat by its time integration.

We note as α the ratio $Q/Q_{infinite}$, where Q is the heat produced at a given time and $Q_{infinite}$ the heat that would be produced in a complete hydration of cement. This ratio is generally used to express the hydration degree at a given time. The value $Q_{infinite}$ is calculated from the enthalpies of the hydration reactions and the proportion of the constituents. For the used cement formulation, $Q_{infinite}$ is evaluated to be 483 J/g of cement.

The dissipated heat power as a function of time in milliwatts per gram of cement and the hydration degree α obtained after time integration of the dissipated power and normalization by $Q_{infinite}$ are plotted in Fig. 1.

Although α is an average indication for the whole set of exothermic reactions, this reactional parameter provides us with another basis of interpretation of aggregation and structuration mechanisms in parallel with the analysis versus time. We can then analyze the kinetics of evolution of the mechanical properties as given by ultrasonic spectroscopy and shrinkage measurements, either versus time or versus the amounts of reacted matter.

2.3. Autogeneous shrinkage determination

The autogeneous shrinkage is obtained by hydrostatic weight measurement [8]. Approximately 80 g of fresh concrete are sealed under vacuum in a thin rubber container just after mixing. The watertight rubber container suits the volume variation of the concrete specimen. This container is placed in a thermoregulated bath at 20°C within ±0.02°C and its weight is measured by a scale with a precision of 1 mg linked by a serial RS 232 line to a computer that calculates the volume variation inducing the Archimedean weight variation. A measure is made every 30 s. This relatively high measurement rate allows a redundancy used to decrease the noise variance on the weight measurement and on its derivative versus time.

2.4. Acoustical setup

An acoustic spectroscopic equipment has been used to investigate the evolution of the setting and hardening of concrete [9–11]. Both reflection and transmission of ultrasonic waves have been studied. The technique used short pulses of 1–2 μs duration, which were analyzed in the time and in the frequency domain (after Fourier analysis of the ultrasonic pulses). Broad band longitudinal and shear wave transducers centered at 0.5 MHz were used.

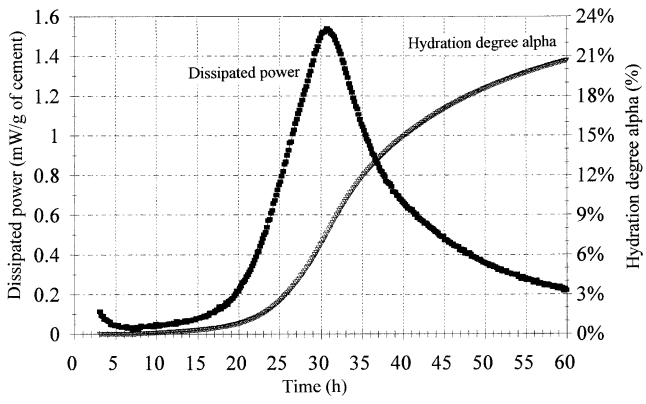

Fig. 1. Dissipated power and hydration degree α versus time.

The cement is located in a Plexiglass cell shaped as a pill-box with a 12-cm diameter and 2-cm height enclosed by 2-cm-thick walls. Two pairs of transducers are fixed on the Plexiglass walls, one pair of longitudinal transducers facing each other, the other for shear waves. Four signals are analyzed: the transmitted longitudinal through the Plexiglass walls and the concrete, the reflected signal by the first interface Plexiglass–cement, and the transmitted and reflected shear signals. The ultrasonic cell is placed in the thermoregulated bath at 20°C. A thermocouple gives the temperature of the concrete, another checks the temperature of the bath.

The measurements are performed every 5 min during 60 to 80 h. A signal analysis program performs the analysis of the several hundred signals obtained; it extracts the reflection and transmission coefficients of the concrete as functions of frequency all along the setting and hardening. It gives also the velocities and amplitudes of the signals from which we can deduct the viscoelastic coefficients and the attenuation in the medium.

3. Results and discussion

In Fig. 2a, the relative volume variation $\Delta V/V$ and its time derivative are presented versus time. Using the evolution curve of Fig. 1, this shrinkage can also be presented versus α (Fig. 2b).

The shrinkage evolution versus time in Fig. 2a leads us to identify two main regimes separated by hour 27 where the shrinkage starts again after a slowing period. The examination of the derivative allows the identification of three periods in the first regime: (before hour 10, between hours 10 and 16, and between hours 16 and 27) and two periods in the second regime (between hours 27 and 32, and after hour 32).

In Fig. 2b, the same events may be observed: hour 16 corresponds to an abrupt change of the shrinkage slope at $\alpha \sim 0.45\%$, hour 27 corresponds to $\alpha \sim 3.5\%$ and hour 32 corresponds to $\alpha \sim 10.0\%$.

We may find in the evolution of the ultrasonic shear and longitudinal waves reflection coefficient moduli (respectively shear and longitudinal reflection coefficients, in Fig. 3a and b) the mechanical and structural information about the same events. Hour 10 is visible as a small decrease of the derivative of the shear reflection coefficient at 125 kHz (Fig. 4). A sharp bend of the shear reflection coefficient and its derivative (Figs. 3a and 4) at the lower frequency (125 kHz) occurs at hour 16. After a minimum corresponding to the impedance matching between the paste and the Plexiglas wall, the frequency dependence of the reflection coefficient vanishes in Fig. 3a; the junction of the curves occurs slightly before hour 27. We can reasonably think that experiments performed at higher frequencies would lead to a later junction, nearer hour 27. Furthermore, this hour sees the beginning of the leveling at a near-zero value of the phase curves at the higher frequencies (Fig. 5). At hour 32, shear and longitudinal reflection coefficients evolutions calm down.

We now discuss in more detail the mechanisms.

Before hour 10, the variation of the shrinkage rate is important and no ultrasonic transmitted waves are detected. The shear reflection coefficient (Fig. 3a) remains equal to 1 telling us that the medium possesses a zero shear acoustic impedance. This means that the medium does not have an elastic or viscous shear modulus. Therefore, a shear wave cannot propagate in the medium and in the ultrasonic frequency range used here, the viscosity is so low that it is unable to lower the reflection coefficient from its maximum value of 1.

Nevertheless, before hour 10, the longitudinal reflection coefficient (Fig. 3b) has begun its decrease from an initial value of less than 1. This means that a longitudinal wave can be inserted in the medium till the beginning, with a better insertion for lower frequencies. This decrease of longitudinal reflection coefficient is concomitant to an important shrinkage (Fig. 2a) without any detectable α (Fig. 1). It is probably due to a continuous short-range reorganization with a stronger interaction between solid particles well detected by the longitudinal reflection coefficient.

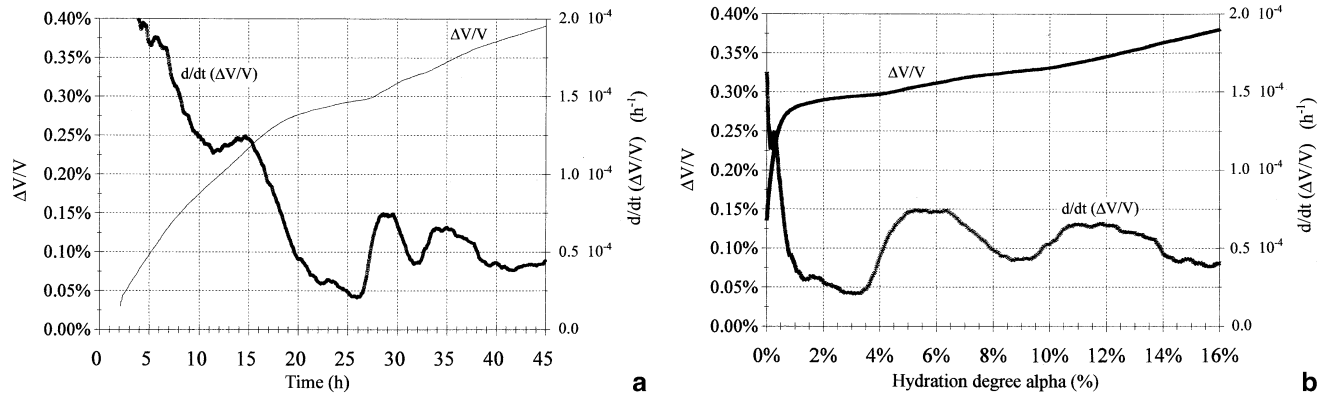

Fig. 2. (a) Relative volume variation and its time derivative versus time. (b) Relative volume variation and its time derivative versus hydration degree.

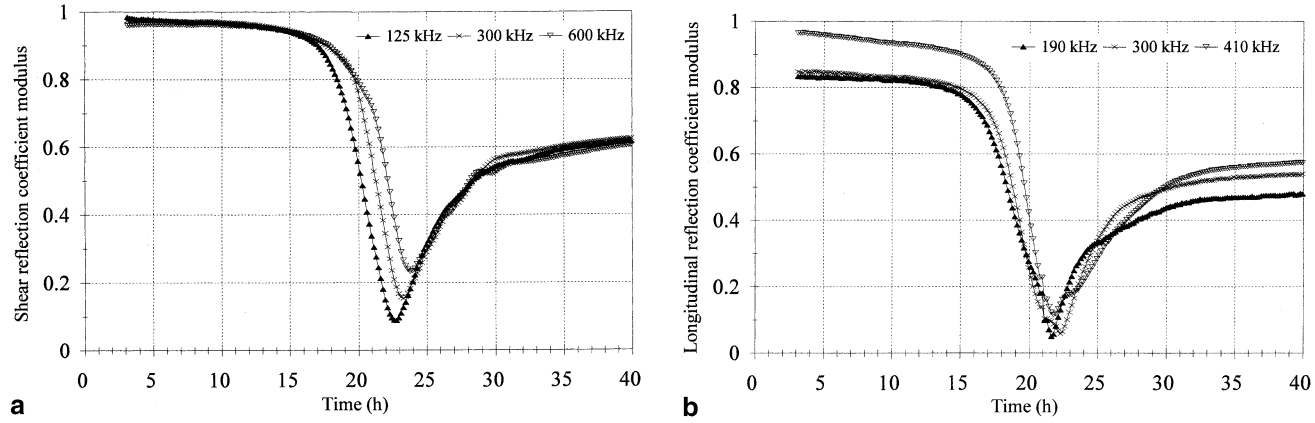

Fig. 3. (a) Shear reflection coefficient modulus versus time. (b) Longitudinal reflection coefficient modulus versus time.

The observed values of the longitudinal reflection coefficient range between 0.8 and 1 according to the frequency. A value of longitudinal reflection coefficient equal to 0.8 would lead to a velocity of 140 m/s.

An estimation of the minimum longitudinal wave velocity given by Wood's formula [12] of sound velocity in a suspension of cement particles in water leads to an estimation of a velocity nearly equal to 1490 m/s in the case where the space between the solid particles is filled with water. This velocity would lead to a value of the longitudinal reflection coefficient of 0.34.

This discrepancy means that at the beginning, the solid particles are not sufficiently coupled by water; the reorganization of powder particles in the water during the first period will cause a better mechanical coupling between particles resulting in a better sound conduction. As it is seen in Fig. 3b, the evolution of the longitudinal reflection coefficient at high frequencies is more sensitive to this phenomenon. In this first period, the results of longitudinal waves are that there is an increasing number of contacts between particles but without creation of bonds which would be detected by shear wave measurements.

It is generally admitted [13] that two physical mechanisms occur during the dormant period: a progressive penetration of water into cement aggregates and a physical shrinkage due to the Van der Waals forces between particles which are more effective for lower w/c ratios [14]. The former can explain the fact that after an initial inability to carry ultrasonic longitudinal waves, the penetration of water between particles leads progressively to a better sound conduction. The latter can explain the important early phase shrinkage and partly the better sound conduction by the medium which is made easier by the increasing close proximity of particles.

At hour 10, the shrinkage derivative (Fig. 2a) stops its decrease and becomes stationary. We note on the calorimetric curve that the thermal activity has begun at hour 7 indicating hydrate formation. The leveling of the derivative results from a compensation: the initial shrinkage derivative which continues to diminish with time and the increase of the shrinkage derivative induced by the exothermic reactions which form hydration products with lower specific volumes. So after hour 10 an increasing part of the shrinkage can be attributed to the exothermic hydrates formation, which becomes the major contribution at hour 15. Further-

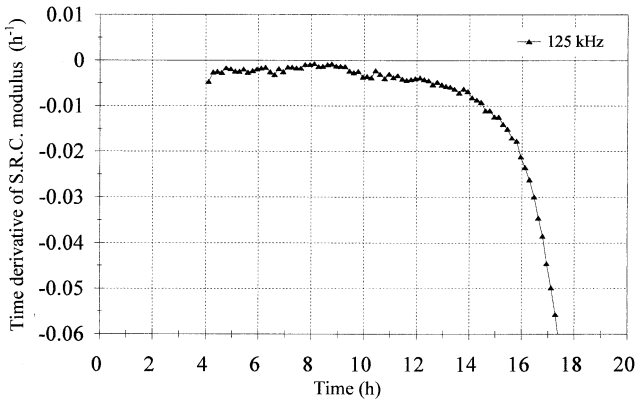

Fig. 4. Time derivative of the shear reflection coefficient versus time.

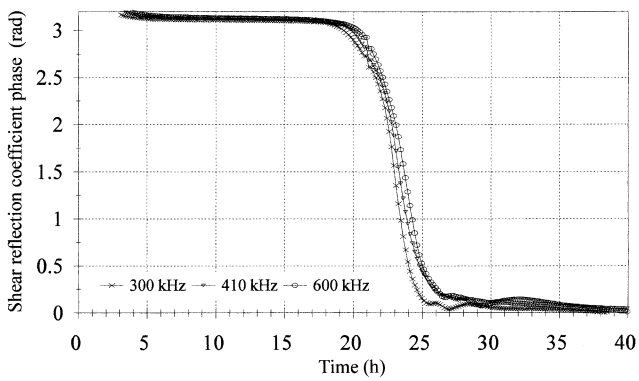

Fig. 5. Shear reflection coefficient phase versus time.

more, between hours 10 and 16, the shear reflection coefficient decreases slowly (Fig. 3a), expressing the growth of aggregates. Then the behavior of the material is that of an unstructured paste in which viscosity increases regularly. Nevertheless, the growth of aggregates and the quality of contacts is not sufficient to allow, in our frequency range of evaluation, any detection of a transmitted shear sound wave from one side to the other side of the sample (Fig. 6a). The percolation of contacts between the particles is not established by the detection of any propagation through the sample but indirectly by the fact that at hour 10 the shrinkage is impaired by the agglomeration of the sample as a whole (Fig. 2a). This state at hour 10 can be identified as a percolation point (P point).

For cement pastes or concrete with high water content, a swelling of the sample was observed in the first main period [15,16]. This swelling is generally linked with the formation of portlandite. It has been shown that portlandite formation is very low or practically absent in RPC. On the other hand, if significant amounts of portlandite were formed in the early stage of the reactions, the calorimetric curve (Fig. 1) would exhibit an exothermic pozzolanic reaction with silica fume after the main calorimetric peak around hour 45 which is actually absent here.

In any case, the portlandite formation would only contribute here to reduce the shrinkage and does not act in swelling.

The increasing rate of shrinkage between hours 10 and 16 corresponds to a period where the bringing together of particles is large.

At hour 16, the shrinkage time derivative (Fig. 2a) begins to decrease even if the chemical hydration continues to increase (Fig. 1). This abrupt shrinkage time derivative decrease is probably induced by the locking of the solid skeleton at hour 16, which impedes further plastic rearrangements of the material. One can deduce that at hour 16, the medium has globally no degree of freedom of the largest particles remaining: The name of 'isostatic' point (I point) is then used in this paper by analogy with a structural mechanics term. Nevertheless, smaller interstitial particles may remain mechanically uncoupled inside the frame.

Simultaneously, we note a blunt variation of the shear reflection coefficient modulus (Fig. 3a) at the lower frequencies favored by the full contact having occurred between solid particles. At this hour, transmitted waves begin to be detected, too (Fig. 6a and b). The extrapolation of shear wave results in Fig. 6a, using a log–log plot which is not represented here, leads to an estimation of the beginning of the shear transmissivity at hour 16, which approximately corresponds to the I point. A low-frequency longitudinal transmitted wave is detected slightly before hour 17 (Fig. 6b).

Between hours 16 and 27, the shrinkage is more and more hindered by the increased number of bonds which form a network through the volume of paste. The sharp decrease of shear and longitudinal reflection coefficient modulus comes in this sample with a large frequency dependence, the lower frequency reflection coefficients decreasing sooner. In the first approximation, in this period, the propagation in the medium has the frequency characteristics to that of an elastic wave in a mass-spring chain.

During the material evolution between hours 16 and 27, more and more small interstitial clusters will be linking to the main framework; the effective springs elastic constant in the skeleton will increase continuously causing an evolution of the frequency dependence and an increase in the cutoff frequency.

At hour 27, the bundle of the reflection coefficient curves (Fig. 3a and b) has converged. As expressed earlier, the convergence of the shear and longitudinal reflection coefficient curves occurs slightly before hour 27, due to the limitation of the frequency band of the ultrasonic signals used. As the phase curve of shear reflection coefficient levels to zero at hour 27 (Fig. 5), one can deduce that the

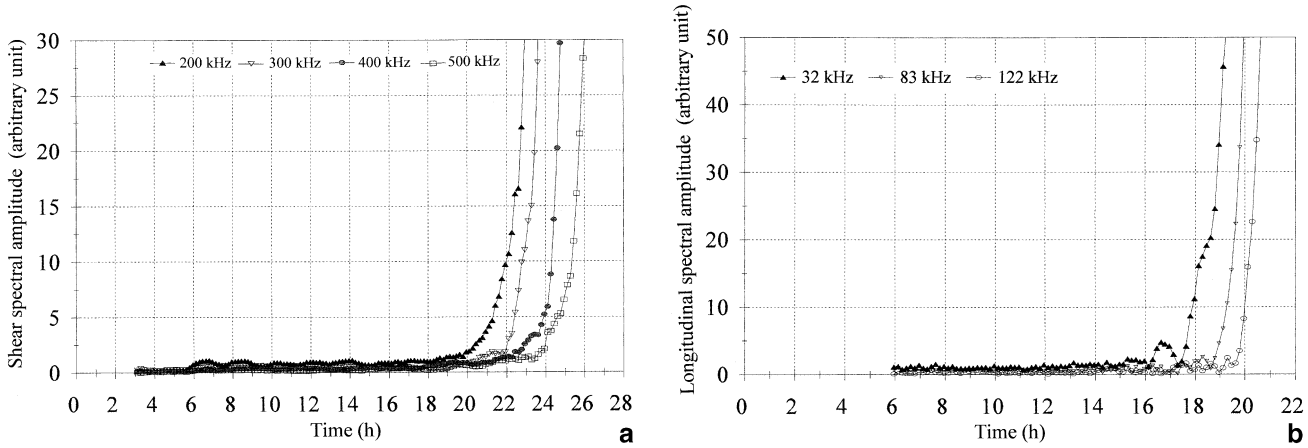

Fig. 6. (a) Shear spectral amplitude versus time. (b) Longitudinal spectral amplitude versus time.

frequency cutoff tends to infinity. At hour 27, the material reaches its complete hyperstatic configuration (H point). The number of overabundant links is important, making the resonant frequencies of the structure very high.

From hour 27 the shear and longitudinal reflection coefficients do not depend anymore upon frequency. Nevertheless, the viscoelastic coefficients continue to evolve, as seen on the sharp increase of the shear and longitudinal reflection coefficients in Fig. 3a and b, due to an intense chemical activity (Fig. 1) which contributes to the creation of new bonds and makes the material more and more 'hyperstatic' at different scales.

The shrinkage is reactivated at hour 27 (Fig. 2a) for, at least, two reasons: first, the chemical reaction is highly activated (calorimetric peak) and contributes to an acceleration of the chemical component of the shrinkage (Le Châtelier shrinkage) and, second, the capillary forces are activated by the diminution of free water used in the intense chemical reaction. At this stage, the capillary forces fully develop and induce the restart of the shrinkage at this hour. As the material is now totally connected, the shrinkage forces will necessarily affect the matrix integrity. Beyond hour 27, the observation of the derivative curve of shrinkage leads to the identification of two bumps in the representation versus time and more clearly versus α. This can correspond to the following phenomena: During the first stage, the material must adapt to the new situation in releasing the capillary forces by microcracking, but as the material is highly chemically active, these microcraks may rapidly heal. As a consequence of the release of capillary forces by microcracking and self-healing, the shrinkage goes on with a slight incurvation. One can imagine that the microcracking occurring during the second bump on the shrinkage rate may not heal as easily as the first one.

Finally, let us discuss the different stages of structure development of this ultra-high-performance concrete on the plots (Fig. 7) of the elastic moduli (Young's and bulk moduli, Poisson's ratio) measured at 190 kHz obtained from the transmission measurements of the longitudinal and shear waves.

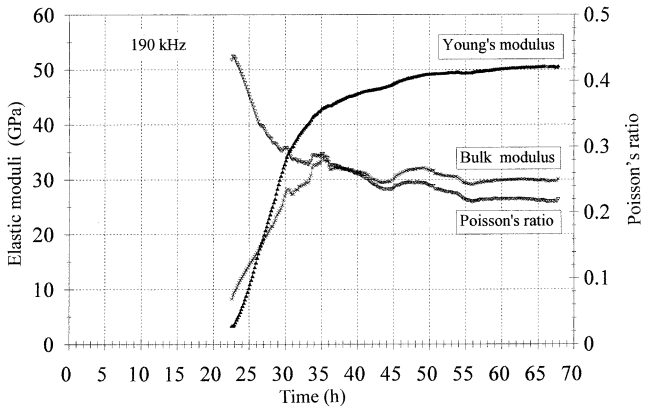

Fig. 7. Elastic moduli at 190 kHz versus time.

Evidently, no information can be extracted before hour 20 because of the strong attenuation of the medium at this frequency before that hour. Nevertheless, different periods can be observed.

- After hour 20, the increase of the connected clusters in the medium leads to a rapid evolution of both Young's and bulk moduli and decrease of Poisson's ratio.
- At hour 27 (H point), the global structuration of the medium provokes a modification of the slope of the Young's modulus curve, which induces a slight bend of that curve. It may be noted that at this state, bulk and Young's moduli have the same value.
- After the H point, the multiplication of the connections continues to cause a rapid increase of both moduli.
- After the J point, the Young's modulus continues to increase slowly, probably now due to a slow pore filling mechanism when the variation of the bulk modulus is no longer appreciable within the time range of the experiment.

4. Conclusions

A combined analysis of the structure development of an RPC sample using three different techniques of analysis has provided a detailed picture of the different mechanisms involved in the setting dynamic of the material and its successive states of structure development.

Three areas for further research appear from the gained perspective.

- In the field of civil engineering, the understanding of the microcracking dynamics, the determination of the right time of origin of the damaging shrinkage evaluation and the optimization of the in-field shuttering process.
- In the field of shaping of cement-based materials, the knowledge of the main structuration states leads to a better control and optimization of the manufacturing process.
- In the field of elaboration of new concrete with specific microstructural shapes, which would be obtained by the monitoring and control of the duration of the successive structuration stages.

References

[1] P. Richard, M. Cheyrezy, Composition of reactive powder concretes, Cem. Concr. Res. 2 (1995) 1501–1511.
[2] A. Feylessoufi, F. Villieras, L.J. Michot, P. De Donato, J.M. Cases, P. Richard, Water environment and nanostructural network in a reactive powder concrete, Cem. Concr. Compos. 18 (1996) 23–29.
[3] E. Sauzeat, A. Feylessoufi, F. Villieras, J. Yvon, J.-M. Cases, P. Richard, Textural analysis of a reactive powder concrete, Proc. 4th Int. Symp. on Utilization of High-Strength/High-Performance Concrete, Paris, France, 1996, pp. 1359–1365.
[4] A. Feylessoufi, M. Crespin, P. Dion, F. Bergaya, H. Van Damme, P. Richard, Controlled rate thermal treatment of reactive powder concretes, Adv. Cem. Based Mater. 6 (1997) 21–27.
[5] M.P. Faugère, M. Crespin, P. Dion, F. Bergaya, A. Feylessoufi, H. Van Damme, Influence of heat treatment kinetics on calcium silicate

hydrates phase evolution, in: P. Colombet, A.-R. Grimer, H. Zanni, P. Sozzani (Eds.), Magnetic Nuclear Resonance Spectroscopy of Cement Based Materials, Springer-Verlag, Berlin, 1998, pp. 217–225.

[6] L. Gatty, S. Bonnamy, A. Feylessoufi, H. Van Damme, P. Richard, Silica fume distribution and reactivity in reactive powder concretes, Proc. Sixth CANMET/ACI Int. Conf. on Fly Ash, Silica Fume, Slag and Natural Pozzolans in Concrete, Bangkok, Thailand, 1998, pp. 931–953.

[7] V. Morin, F.C. Tenoudji, C. Vernet, A. Feylessoufi, P. Richard, Ultrasonic spectroscopy investigation of the structural and mechanical evolutions of reactive powder concretes, Proc. Int. Symp. on High Performance Concrete and Reactive Powder Concrete, Sherbrooke, Canada, 1998, pp. 119–126.

[8] E. Tazawa, S. Miayazawa, T. Kasai, Chemical shrinkage and autogeneous shrinkage of hydrating cement paste, Cem. Concr. Res. 25 (1995) 288–292.

[9] F. Levassort, F. Cohen Tenoudji, Rapport DEA Acoustique Physique, University of Paris VII, Paris, 1991 (ed.).

[10] A. Boumiz, C. Vernet, F.C. Tenoudji, Mechanical properties of cement pastes and mortars at early ages, Adv. Cem. Based Mater. 3 (1996) 94–106.

[11] V. Morin, F.C. Tenoudji, C. Vernet, Study of the viscoelastic behaviour of cement pastes at early ages with ultrasonic waves in echographic mode, Proc. Second RILEM Workshop on Hydration and Setting, Dijon, France, 1997.

[12] A.B. Wood, A Textbook of Sound, Macmillan, New York, 1941 (ed.).

[13] J. Baron, R. Sauterey, Le béton hydraulique, Presses des Ponts et Chaussées, Paris, 1982 (ed.).

[14] G.D. De Haas, P.C. Kreijger, E.M.M.G. Niël, J.C. Slagter, H.N. Theissing, E.M. Theissing, M. Van Wallendael, The shrinkage of hardening cement paste and mortar, Cem. Concr. Res. 5 (1975) 295–319.

[15] T.C. Powers, The Properties of Fresh Concrete, Wiley, New York, 1968 (ed.).

[16] T.C. Powers, Aspects fondamentaux du retrait du béton, Rev. Mater. Constr. 545 (1961) 79–85.